Available online at www.sciencedirect.com
ScienceDirect
Journal of Power Sources 172 (2007) 782–789
JOURNAL OF POWER SOURCES
www.elsevier.com/locate/jpowsour

Degradation of silicone rubber under compression in a simulated PEM fuel cell environment

Jinzhu Tan [a,1], Y.J. Chao [a,*], Xiaodong Li [a], J.W. Van Zee [b]

[a] *Department of Mechanical Engineering, University of South Carolina, 300 S. Main, Columbia, SC 29208, USA*
[b] *Department of Chemical Engineering, University of South Carolina, Columbia, SC 29208, USA*

Received 28 March 2007; received in revised form 10 May 2007; accepted 11 May 2007
Available online 18 May 2007

Abstract

Long-term stability and durability of gaskets in Polymer Electrolyte Membrane (PEM) fuel cell is critical to both sealing and the electrochemical performance of the fuel cell. In this paper, the time-dependent chemical and mechanical degradation of silicone rubber, which is one of the potential gasket materials for PEM fuel cells, was investigated. Test samples were subjected to a constant compressive load to simulate the actual loading on seals and soaked in a simulated PEM fuel cell environment. Based on actual PEM fuel cell operation, two temperatures 60 °C and 80 °C were selected and used in this study. The optical microscopy was used to reveal the topographical changes on the sample surface. Atomic absorption spectrometer analysis shows that silicon, calcium and magnesium were leached from the material into the soaking solution. Attenuated total reflection Fourier transform infrared (ATR-FTIR) spectroscopy was employed to study the surface chemistry of the silicone rubber before and after exposure to the test environment. The ATR-FTIR results indicate that the surface chemistry changed significantly via de-crosslinking and chain scission in the backbone for the material over time. The microindentation test was used to assess the change of mechanical properties of the material before and after exposure to the environment. It was found that the mechanical properties of the silicone rubber material changed significantly and both the temperature and the exposure time have direct effect on the stiffness of the material.

Keywords: Fuel cell; Silicone rubber; Degradation; Compressive load; Attenuated total reflection Fourier transform infrared spectroscopy; Microindentation

1. Introduction

Polymer Electrolyte Membrane (PEM) fuel cell stack requires elastomeric gaskets and seals in each cell to keep the reactant gases (hydrogen and oxygen) within their respective regions. The elastomeric gaskets used as seals in fuel cell are exposed to acidic environment, humid air and hydrogen, and subjected to mechanical compressive load. If any gasket degrades or fails in PEM fuel cells, the reactant gases (H_2 and O_2) can leak overbroad or mixed with each other directly during operation or during standby. It affects not only the overall operation reducing the efficiency of the performance but also poses safety concern. In addition, gasket as seal in fuel cells must be flexible to allow compression of the stack in order to keep intimate contact between all components in the cells. If any gasket degrades (e.g. hardening), the gasket may lose its functionality, thus affecting the durability of the fuel cell operation. Furthermore, the leached materials (e.g. calcium) from the gasket can poison the cell and reduce the fuel cell voltage and durability. Understanding the seal degradation mechanisms is a scheduled, funded task within the Department of Energy plan for the development for PEMFCs [1]. The magnitude of the opportunity is evident when one realizes that 0.4 km of seal is required for a 100 kW fuel cell operating at present-day power densities of 0.7 W cm^{-2} (estimated for a stack with 200 cells of 714 cm^2 active area).

Silicone rubber materials are widely used as sealing materials in many industrial applications including fuel cells because of their low cost and ease in fabrication [2,3]. There are many published reports regarding the degradation of silicone rubbers [2–19] in various environments. For example, Zhu et al. [6] studied the surface degradation of silicone rubber exposed to corona discharge. Gustavsson et al. [14] reported the results of aging of

* Corresponding author. Tel.: +1 803 777 5869; fax: +1 803 777 0106.
E-mail address: chao@sc.edu (Y.J. Chao).
[1] Permanent address: College of Mechanical and Power Engineering, Nanjing University of Technology, Nanjing, Jiangsu 210009, China.

0378-7753/$ – see front matter © 2007 Elsevier B.V. All rights reserved.
doi:10.1016/j.jpowsour.2007.05.026

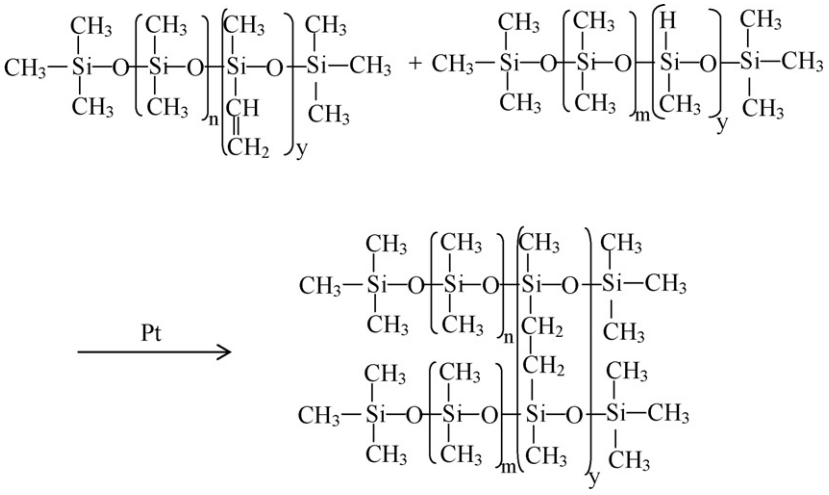

Scheme 1. The crosslinking reaction for the silicone rubber.

silicone rubber under ac or dc voltages in a coastal environment. A review on the effects and degradation process of silicones in the environment can be found in Graiver et al. [15]. Tan et al. [16,17] reported the degradation of elastomeric gasket materials in a simulated fuel cell environment. Although there is a substantial literature concerning the degradation of silicone rubber, few results were reported for the degradation and its mechanisms of silicone rubber materials under compressive load in PEM fuel cell environment.

In this paper, the chemical and mechanical degradations of a silicone rubber material under a constant compressive load in a simulated fuel cell environment were investigated. The aim of the present study is to investigate the degree of degradation and its mechanisms for the silicone rubber samples subjected to compressive load and exposed to the environment. The compressive load is to simulate the actual loading applied to the seal/gasket during service. An accelerated durability test (ADT) solution and two temperatures were used in the short-term, accelerated aging tests of the gasket material. Surface changes were examined using optical microscopy and weight loss was monitored on the samples at selected exposure times. The chemical degradation on the surface of the silicone rubber after exposure to the simulated fuel cell environment over time was studied using ATR-FTIR spectroscopy. Atomic absorption spectrometry was also used to identify the chemicals leached from the silicone samples into the soaking solution. The microindentation test method was used to assess the change of mechanical properties of the material before and after exposure to the environment.

2. Experiments

2.1. Material and simulated fuel cell environment

The material used in this study is the elastomeric gasket material, silicone rubber, which is one of the commercially available gasket materials. The rubber is a two-part formulation liquid injection molded material. It mainly contains polydimethylsilicoxane with vinyl functionalities in part I and polydimethylsilicoxane with hydrosilylation functionalities in part II. The parts I and II (1:1) were combined and heated to crosslink under the platinum catalyzed reaction. The crosslinking mechanism is hydrosilylation. The chemical structures of the material used in our study are shown in Scheme 1. The possible reaction mechanism of crosslinking is also included in Scheme 1. The fillers inside the material mainly include silica, quartz and calcium carbonate.

An ADT solution for short-term accelerated aging tests was used as the simulated fuel cell environment for this study. Forty-eight percentage of HF and 98% H_2SO_4 were dissolved in balance reagent grade water to make the ADT solution. The final composition of the ADT solution is 1 M H_2SO_4, 10 ppm HF and reagent grade water having 18 MΩ resistance as the exposure medium.

The test temperatures were 80 °C and 60 °C, which are close to the operating temperatures of actual PEM fuel cells.

2.2. Aging and characterization methods

Rectangular-shaped specimens from the silicone rubber material were prepared. The dimensions of the samples are 65 mm in length, 10 mm in width, and 1.0 mm in thickness. The samples were sandwiched between two Plexiglas plates and applied a dead weight 76 N giving a pressure of 0.12 MPa to the test sample. As shown in Fig. 1, the sample and the fixture were placed in a larger polypropylene bottle containing ADT solutions. The larger bottle was then put in an oven with 80 °C and 60 °C for 1–26 weeks. The samples were taken out every one or 2 weeks for examination. The change in weight over time was monitored on the samples. The surface conditions of the samples were examined using optical microscope (Leco, OLYMPUS PME-3) at selected times.

The ATR-FTIR spectroscopy was performed on the surface of the samples using a Nexus Model 670 Instrument (Nicolet Instrument Corporation) and run with 128 scans at a resolution of 4 cm^{-1}. The infrared radiation (IR) penetrates the surface of the test sample to approximately 1 μm. In order to avoid the effect of the remaining ADT solution on the sample surface on

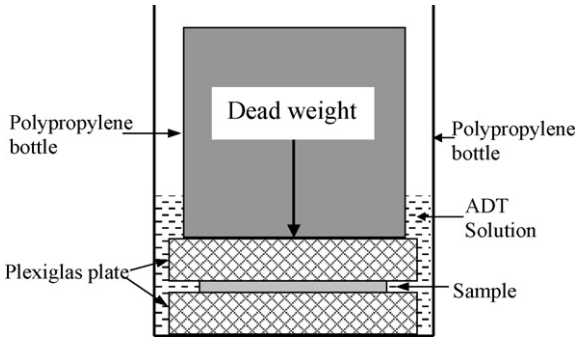

Fig. 1. Schematic representation for tests under the compressive load.

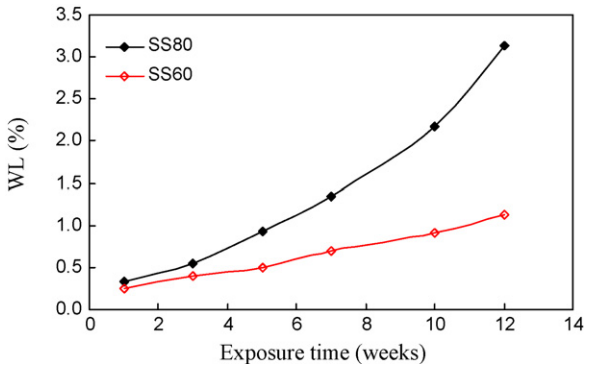

Fig. 2. Weight loss with exposure time from the test samples at 60 °C and 80 °C.

the ATR-FTIR results, the surface of the sample was cleaned using reagent grade water having 18 MΩ resistance to remove the excess acids and made dry at room temperature before the ATR-FTIR analysis.

In addition, the solution exposed to each sample was taken out at selected time and analyzed for leachants using atomic absorption spectrometry (Perkin-Elmer 3300).

In order to assess the mechanical properties of the samples before and after exposure to the environment under the compressive load, microindentation tests were performed on the samples before the test and after 12 weeks. The microindenter (CETR, Campbell CA) monitors and records the load and displacement of the indenter. The tip of the indenter is a stainless steel ball with a radius of 1.98 mm. The instrument has a force resolution of 0.5 mN and a displacement resolution of 0.1 μm. In all analyses, the materials without exposure to the ADT solution were also characterized for comparison.

3. Results and discussion

3.1. Weight change

The samples were taken out from the test chamber at selected times. The surface of the sample was carefully cleaned using reagent grade water having 18 MΩ resistance to remove the excess acids and made dry at room temperature before the weight change was monitored. The percent weight loss, WL, was calculated using the following equation:

$$\mathrm{WL} = \frac{W_1 - W_2}{W_1} \times 100 \quad (1)$$

where W_1 is the initial weight of the sample in air and W_2 is the weight of the aged sample in air.

Fig. 2 shows the change of weight over time at the two temperatures. In the figure, SS80 and SS60 represent the silicone material at 80 °C and 60 °C, respectively. It is shown that weight loss increased with exposure time for the samples. The weight loss for the sample at 80 °C was more than that at 60 °C representing the temperature effect. The trend of weight loss in this study is similar to those in our previous work [16,17] in which samples were not subjected to mechanical compressive load.

Test results of percent weight loss per square centimeter are listed in Table 1. Data from our pervious study [17] which had no mechanical load applied to the samples are also listed in Table 1 for comparison. At 80 °C, very similar results are obtained for the two sets of data. However, a significant difference between the two sets of data, roughly 15–18 times, is observed for those samples tested at 60 °C. It indicates that the mechanical compressive load is more important in weight loss at 60 °C while the temperature effect becomes dominant at 80 °C, which masked the effect due to the mechanical load.

Overall, it is concluded from this study that (a) temperature has a significant effect on the weight loss such that the silicone has more weight loss at higher temperature, (b) the mechanical compressive load accelerated the weight loss at lower temperature, i.e. 60 °C, and (c) the effect due to mechanical compressive stress at the higher temperature 80 °C is not observed.

3.2. Microscopy

Optical microscopy was used to visually observe the degradation of the surface of the material in our study. Fig. 3 shows the optical micrographs from the samples before and up to 26-week exposure to ADT solution at 80 °C or 60 °C under the compressive load. The magnification used was 500×. The photos (a)–(g) are from the surface where the dead weight load is applied and (h)–(k) are from the side surface of the samples where solution was always in contact with the samples. The optical micrographs in Fig. 3(a)–(e) shows the typical surface conditions for the sample before exposure and after 5-week, 10-week, 12-week and 26-week exposure to the ADT solution at 80 °C. The typical optical micrographs from the sample after 12-week and 26-week exposure to the ADT solution at 60 °C are shown in Fig. 3(f) and (g). The typical optical micrographs for the samples before exposure and after 3-week and 12-week

Table 1
Percent weight loss per square centimeter of the test samples

Exposed environment	Exposed time (weeks)			
	3	5	7	10
ADT solution at 80 °C [17]	0.332	0.646	0.935	1.374
ATD solution at 80 °C with compressive load	0.367	0.614	0.898	1.447
ADT solution at 60 °C [17]	0.014	0.022	0.027	0.035
ATD solution at 60 °C with compressive load	0.260	0.331	0.466	0.609

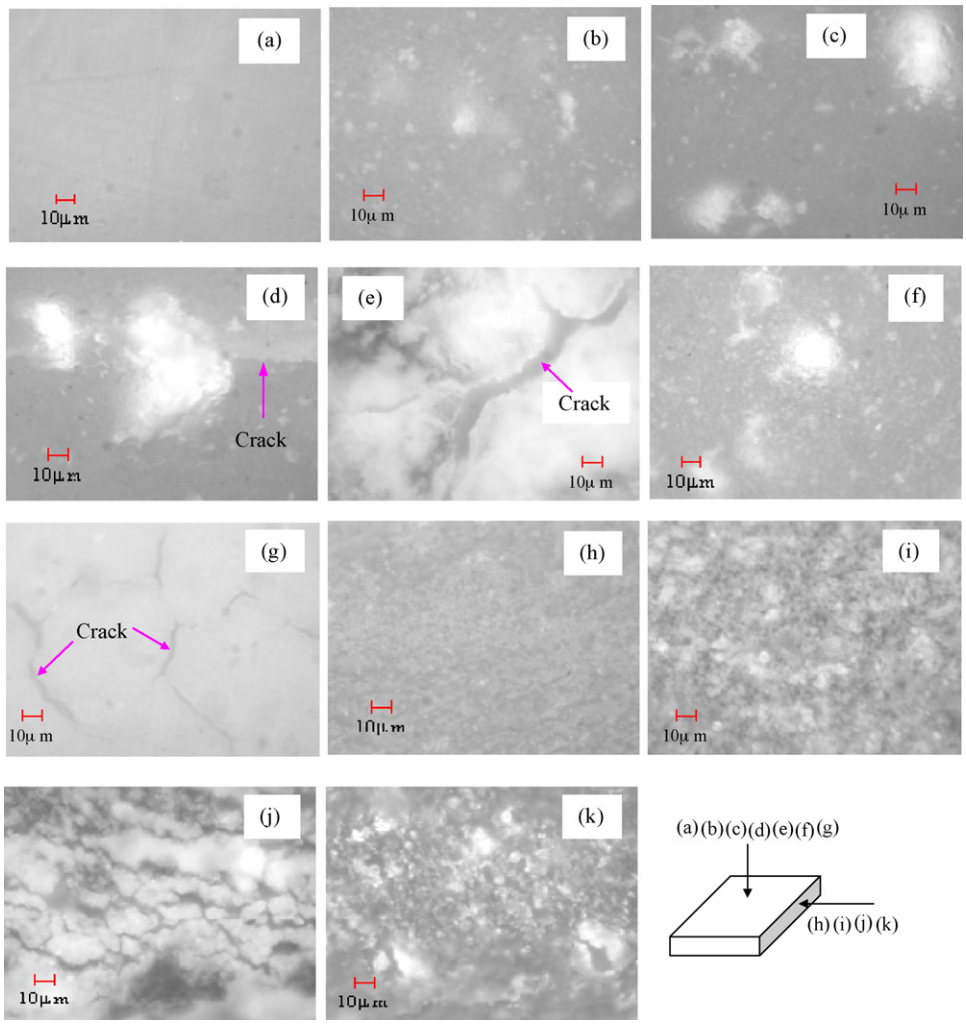

Fig. 3. Optical micrographs of the surface of the test samples where (a)–(g) are from the surface where the dead weight load is applied and (h)–(k) are from the side surface. (a) Before exposure, and after (b) 5-week, (c) 10-week, (d) 12-week and (e) 26-week exposure at 80 °C; (f) 12-week and (g) 26-week exposure at 60 °C; (h) before exposure, (i) 3-week and (j) 12-week exposure at 80 °C; (k) 12-week exposure at 60 °C.

exposure to the ADT solution at 80 °C, and 12-week exposure to the ADT solution at 60 °C are also shown in Fig. 3(h)–(k).

It can be seen from Fig. 3 that the surface conditions of the samples were changed over time from initially smooth to rough, crack appearance and finally crack propagation. The crack size increased with exposure time (see Fig. 3(d) and (e)). The extent of surface damage at 80 °C is more severe compared to 60 °C under identical conditions (see Fig. 3(d) for 80 °C, (f) for 60 °C, (e) for 80 °C and (g) for 60 °C). Furthermore, the extent of damage on the side surface (see Fig. 3(i)–(k)) which has direct contact with the solution is more severe compared to the surface in contact with the applied dead weight (see (b), (d) and (f)).

It can be concluded that (a) the surface topography of the silicone rubber material exhibits time dependent degradation and (b) temperature and exposed medium have significant effect on the degradation.

3.3. ATR-FTIR

ATR-FTIR analysis was performed on the silicone rubber samples before and after exposure to the environment. Figs. 4 and 5 show the ATR-FTIR results for the samples at 80 °C and 60 °C, respectively, up to 12-week exposure.

The strongest and broadest peaks for the unexposed samples (shown in Figs. 4(A-a) and 5(A-a)) are between 1015 cm^{-1} and 1080 cm^{-1} due to the stretching vibrations of Si–O–Si present in the silicone rubber backbone. It can also be seen that the long chain siloxanes have two broad IR peaks near 1015 cm^{-1} and 1080 cm^{-1}. The peaks at 1260 cm^{-1} and 866 cm^{-1} are from the bending vibration of Si–CH_3 and the rocking vibration of of Si–CH_3. The peaks at 2960 cm^{-1} (shown in Figs. 4(B) and 5(B)) are from the stretching vibration mode of CH_3. The peaks near 1418/1415 cm^{-1} (Figs. 4(A) and 5(A)) are from the rocking vibration of –CH_2– as a part of the silicone rubber crosslinked domain. The correspondence bewteen the wavenumber and the vibration mode is from the handbook [20].

The intensity of the peaks between 1015 cm^{-1} and 1080 cm^{-1} decreased sharply after 5-week exposure and almost disppeared after 10-week exposure at 80 °C (see Fig. 4). Similar trends can be seen for the characteristic peaks at 866 cm^{-1}, 1260 cm^{-1} and 1418 cm^{-1} in Fig. 4(A). In Fig. 4(B), similar trend at 2960 cm^{-1} is observed. Simultaneously a group of

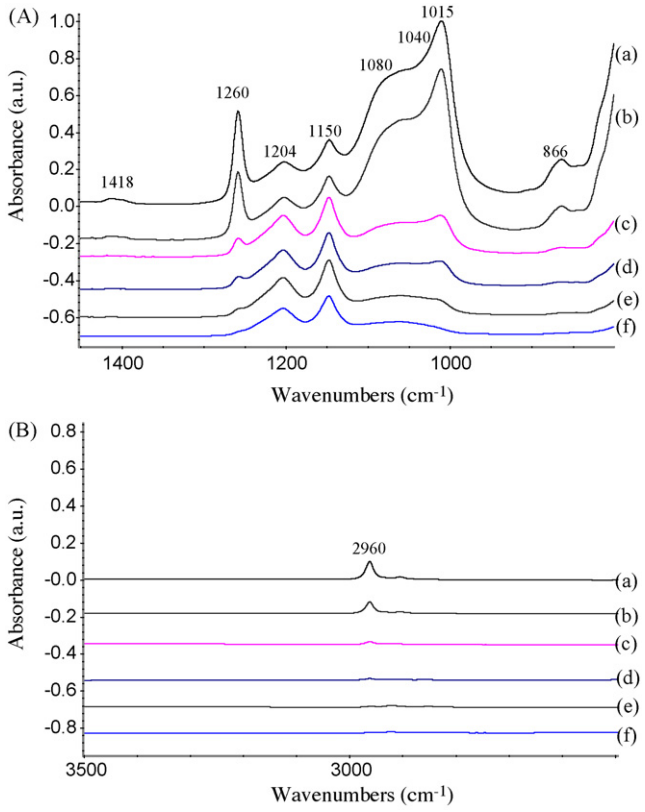

Fig. 4. Comparison of ATR-FTIR test results for the sample exposed to ADT solution at 80 °C and subjected to the compressive load: (a) without exposure, after (b) 3-week, (c) 5-week, (d) 7-week, (e) 10-week and (f) 12-week exposure. ATR-FTIR spectra from (A) 800 cm^{-1} to 1450 cm^{-1} and (B) 2500 cm^{-1} to 3500 cm^{-1}.

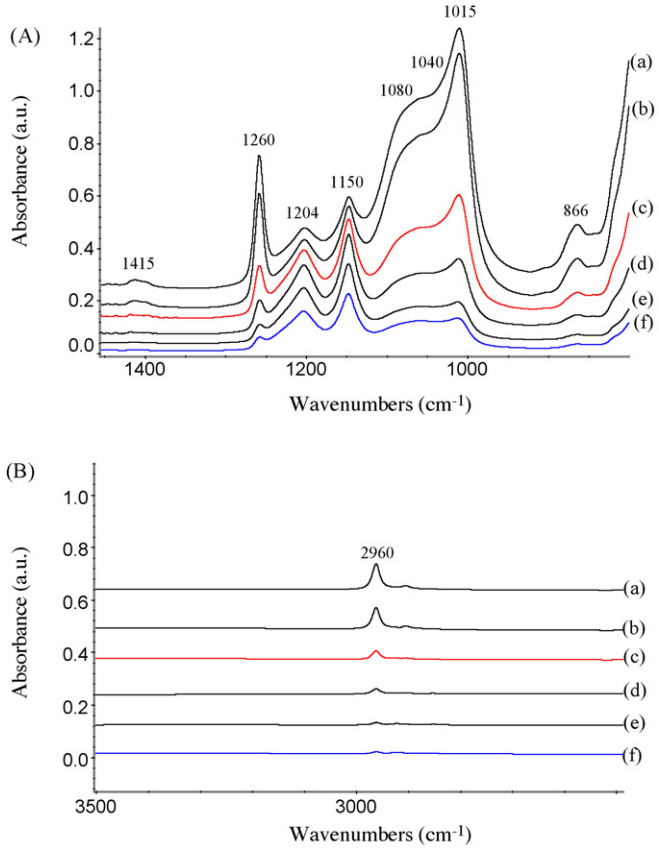

Fig. 5. Comparison of ATR-FTIR test results for the sample exposed to ADT solution at 60 °C and subjected to compressive load: (a) without exposure, after (b) 3-week, (c) 5-week, (d) 7-week, (e) 10-week and (f) 12-week exposure. ATR-FTIR spectra from (A) 800 cm^{-1} to 1450 cm^{-1} and (B) 2500 cm^{-1} to 3500 cm^{-1}.

new peak emerges at the spectrum near 1040 cm^{-1}, which is likely from the stretching vibration of Si–O as a consequence of chemical changes.

The trends observed at 60 °C (Fig. 5) are simlilar to those in 80 °C (Fig. 4). The intensities of the peaks at 1015 cm^{-1} and 1080 cm^{-1}, 866 cm^{-1}, 1260 cm^{-1}, 1415 cm^{-1} and 2960 cm^{-1}, decreased sharply after 5 weeks and then almost disppeared after 12 weeks as shown in Fig. 5. A new peak was emerged at the spectrum near 1040 cm^{-1}, which is likely due to stretching vibration of Si–O as the chemistry changes.

It is observed from this ATR-FTIR study that there are significant chemical changes in rubber backbone and the crosslinked domain for the silicone rubber samples tested in this condition over time. The degradation mechanisms of the silicone rubber could be due to de-crosslinking via hydrolysis of crosslink sites and chain scissoring in the backbone in the test environment. The chemical change in the silicone rubber backbone could be due to the attack of the Si–O–Si by the strong acid (pH < 1), especially Fluoric acid, to form Si–OH. And, then the Si–OH could be converted to Si–O. Although the main chain Si–O–Si in silicone rubber is stable, the Si–O–Si can be atacked/damaged in strong acidic enviroment and this caused significant chemical change [15,18,19,21].

Scheme 2 shows the possible de-crosslinking reactions at crosslink sites of the silicone rubber and combination reactions upon prolonged exposure to the environment. At the crosslinking sites (see Schemes 1 and 2), there exist the bonds of C–C, C–H and C–Si. The bond dissociation energies of C–C, C–H and Si–C are 334 kJ mol^{-1}, 414 kJ mol^{-1} and 301 kJ mol^{-1}, respectively [22,23]. Therefore, the decrease in the intensity of the peak near 1418/1415 cm^{-1} (shown in Figs. 4(A) and 5(A)) as a manifestation of chemical change in the silicone rubber crosslinked domain is most likely due to the damage of the Si–C through the hydrolysis to form Si–OH as shown in Scheme 2. Upon prolonged exposure to the solution, the Si–OH groups could be combined to form the new Si–O–Si and this results in new crosslinkages as shown in Scheme 2.

The decrease of the intensity peak at Si–CH_3 as shown in Figs. 4(A) and 5(A) reflects the chemical change which could be simialr to that at Si–CH_2 in crosslinking sites to form Si–O. The Si–O could then be combined with other Si–O to form the new Si–O–Si. Consequently, the intensity peak at–CH_3 decreased and finlally disappeared in Figs. 4(B) and 5(B). These had caused a decrease in the ratio of C/Si and an increase in O/Si as revealed by our XPS results [16].

3.4. Atomic absorption spectrometry

The atomic absorption spectrometry was employed to analyze the solution to identify potential materials leached from

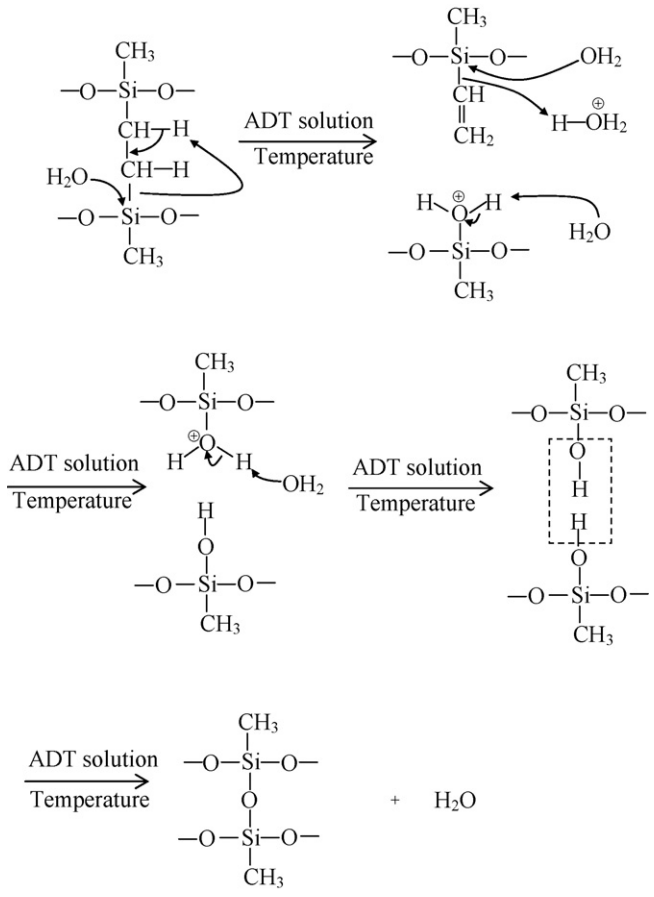

Scheme 2. The de-crosslinking reaction at crosslinked sites of the rubber and combination reaction.

the silicone rubber samples into the soaking solution. Silicon, calcium and magnesium were studied and identified in the solution. Fig. 6 shows the silicon, calcium and magnesium values for the samples exposed to ADT solution at 80 °C and 60 °C at the selected times. It can be seen that the silicon ions have the highest concentration in the solution, followed by calcium and magnesium ions. The concentration of the magnesium ions is very low and near zero after 10-week exposure. The concentration of leached silicon and calcium ions are not negligible however and increased with exposure time and temperature.

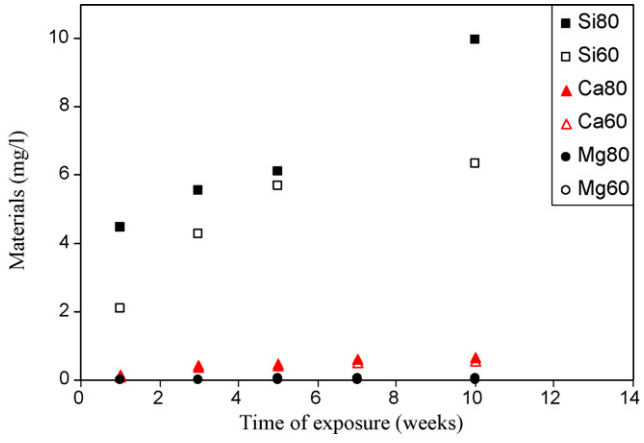

Fig. 6. The silicon, calcium and magnesium values with exposed time for the samples.

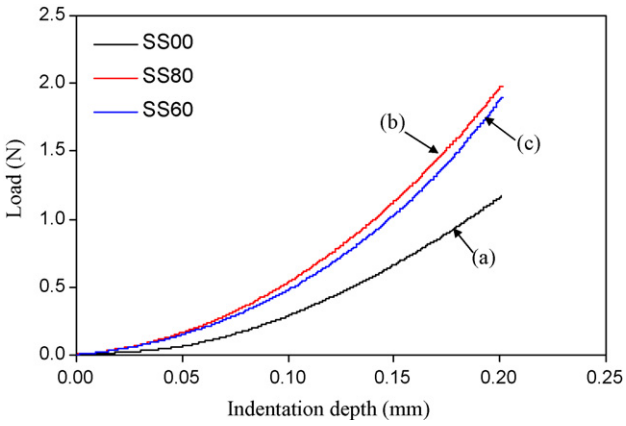

Fig. 7. Load-indentation depth curves for virgin sample (a) and after 12-week exposure at 80 °C (b) and 60 °C (c) at a peak indentation depth of 0.20 mm.

It is noted that fillers in elastomeric compounds are required to enhance the mechanical properties, e.g. tensile strength, hardness, resistance to compression set, for gasket or sealing applications. Our study indicates that when the gasket samples were submerged in the simulated PEM fuel cell solution, some of the fillers such as silicon dioxide and calcium carbonate were attacked by the solution. Consequently, silicon, calcium and magnesium were formed and detected in the soaking solution. These chemicals may be detrimental to the electro-chemical process of PEM fuel cells.

3.5. Microindentation test results

3.5.1. Indentation load

Microindentation load-indentation depth data contains much information from which mechanical properties such as elastic modulus can be determined [24,25]. Fig. 7 shows the indentation load-indentation depth curves for the virgin silicone rubber samples (SS00) and samples after 12-week exposure at 80 °C (SS80) and 60 °C (SS60). Displacement controlled test was used in this test at a peak indentation depth of 0.20 mm. Here, we use the indentation load at the peak indentation depth as a manifestation of the surface hardening of the samples. Fig. 8 shows bar charts of indentation load for the samples before exposure (SS00), and after 12-week exposure at 80 °C (SS80) and 60 °C (SS60) at a peak indentation depth of 0.20 mm. In Figs. 7–9, SS00, SS80 and SS60 represent the unexposed sample, the exposed samples at 80 °C and 60 °C, respectively. From Figs. 7 and 8, the sample exposed to the ADT solution at 80 °C has the largest indentation load, followed by the sample at 60 °C and then the vrigin sample. The results indicate that the samples exposed to the environment and subjected to the compressive load hardened overtime. The extent of the surface hardening at 80 °C is slightly more than that at 60 °C.

3.5.2. Hertz contact modeling

Hertz contact theory was often used to obtain the elastic modulus from the indentation load-indentation depth curves [26].

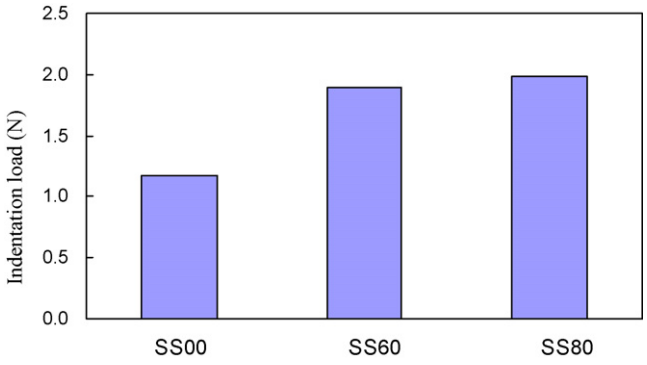

Fig. 8. Bar charts of indentation load for at the peak indentation depth of 0.20 mm for the three samples; virgin (SS00), after 12-week exposure at 80 °C (SS800) and 60 °C (SS60).

Based on the Hertz theory of elastic contact, considering the contact between a rigid sphere (the indenter tip) and a flat surface (the silicone rubber sample), the relationship between the total displacement of both the indenter and sample δ, and the normal load P can be written as [26]:

$$\delta = \left(\frac{9P^2}{16RE^{*2}}\right)^{1/3} \tag{2}$$

where R is the radius of indenter. E^* is a combination of the modulus of the indenter and the sample and can be given by:

$$\frac{1}{E^*} = \frac{1-\nu_{\text{indenter}}^2}{E_{\text{indenter}}} + \frac{1-\nu_{\text{sample}}^2}{E_{\text{sample}}} \tag{3}$$

where E_{indenter} and E_{sample} are the elastic modulus of the indenter and the sample, and ν_{indenter} and ν_{sample} are the Poisson's ratios of the indenter and the sample, respectively. Eq. (2) can be rewritten as:

$$E^* = \frac{3}{4\sqrt{R}} P\delta^{-1.5} \tag{4}$$

When a rigid indenter compresses a soft flat sample like the silicone rubber sample used in this study, δ is the depth of the indentation because the steel indenter's deformation is negligible relative to that of the rubber sample. Based in Eq. (4) and experimental indentation load and indentation depth, the elastic modulus of the sample can be obtained. The elastic modulus and Poisson's ratio of the stainless steel indenter tip were assumed as 2.0×10^{11} Pa and 0.3, respectively [24]. The Poisson's ratio for the silicone rubber sample was assumed as 0.49 [25]. Combining Eqs. (4) and (3), the elastic moduli for the samples were calculated and are shown in Fig. 9. It can be seen that the sample exposed to the ADT solution at 80 °C shows the highest elastic modulus, followed by the sample at 60 °C and then the unexposd sample. The result is in agreement with the indentation load result as shown in Fig. 8. These results indicate that the elastic modulus changed significantly, i.e. the material becomes stiffer, after exposed to the solution and under the compressive load.

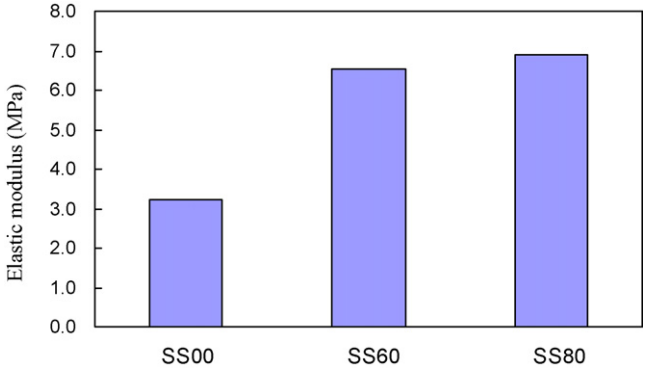

Fig. 9. Elastic modulus of the virgin sample and exposed samples at 80 °C and 60 °C for 12 weeks.

4. Conclusions and future work

Degradation of silicone rubber, a commercial available elastomeric gasket material used as sealing in fuel cell, was studied in a simulated PEM fuel cell solution and under constant compressive load. The following conclusions can be made.

(1) The silicone rubber materials degraded under the test conditions. Temperature has a significant effect on the degradation, i.e. the higher the temperature, the faster the material degraded. The mechanical compressive load accelerated the degradation as seen by weight loss at 60 °C. At the higher temperature 80 °C, the effect due to mechanical compressive stress is not observed in this work.
(2) Optical microscopy shows that the degradation started from increasing surface roughness and finally cracks after exposure to the environment over time.
(3) Atomic adsorption spectrometry identified silicon, calcium and magnisium leached from the gasket materials into the soaking solution. Among them, the silicon ions show the highest concentration in the solution. The concentration of these leached silicon and calcium ions increased with exposure time.
(4) ATR-FTIR results reveal that the surface chemistry changed significantly as an indication of the chemical degradation of the silicone rubber material. The degradation mechanisms of the silicone rubber could proceed via de-crosslinking through hydrolysis of crosslink sites and chain scissoring in the backbone accompanied with the damage of the fillers in the material.
(5) Microindentation test results show that the surface hardening occured and the elastic modulus increased for the exposed samples. The results indicate that chemical degradation or mechanical compressive load affected the mechanical properties.
(6) Current work is to show the fundamental degradation and degradation mechanisms on the silicone rubber material in a simulated PEM fuel cell environment under the compressive load. The chemical degradation and applied compressive load may affect not only the mechanical properties of the material, but also electrochemical performance of the cell and therefore the durability of the PEM fuel cells. Studies on the degradation in mechanical properties of the material

after exposure to the environment under various compressive loads is under investigation and will be reported later.

Acknowledgements

The work was sponsored by the NSF Industry/University Cooperative Research Center for Fuel Cells at the University of South Carolina. Encouragement from the industry partners and financial support from the center were greatly appreciated. The assistance from Xinna Wang and C.C. Stork is acknowledged.

References

[1] Hydrogen, Fuel Cells & Infrastructure Technologies Program Multi-Year Research, Development and Demonstration Plan, updated April 24, 2007, Table 3. 4.15, p. 31, Section 3.4, http://www1.eere.energy.gov/hydrogenandfuelcells/mypp/pdfs/fuel_cells.pdf.
[2] D.A. Dillard, S. Gao, M.W. Ellis, J.J. Lesko, J.G. Dillard, J. Sayre, B. Vijayendran, Proceeding of the Second International Conference on Fuel Cell Science, Engineering and Technology, Rochester, NY, USA, June 14–16, 2004, pp. 553–560.
[3] M. Schulze, T. Knori, A. Schneider, E. Gulzow, J. Power Sources 127 (1-2) (2004) 222–229.
[4] M. Patel, A.R. Skinner, Polym. Degrad. Stab. 73 (3) (2001) 399–402.
[5] L.X. Zhang, S.Y. He, Z. Xu, Q. Wei, Mater. Chem. Phys. 83 (2/3) (2004) 255–259.
[6] Y. Zhu, K. Haji, M. Otsubo, C. Honda, IEEE Trans. Plasma Sci. 34 (4) (2006) 1094–1098.
[7] M. Patel, A.R. Skinner, R.S. Maxwell, Polym. Test. 24 (5) (2005) 663–668.
[8] L. Zhang, Z. Xu, Q. Wei, S. He, Radiat. Phys. Chem. 75 (2) (2006) 350–355.
[9] M. Ehsani, H. Borsi, E. Gockenback, G.R. Bakhshandeh, J. Morshedian, Adv. Polym. Technol. 24 (1) (2005) 51–61.
[10] A. Ghanbari-Siahkali, S. Mitra, P. Kingshott, K. Almdal, C. Bloch, H.K. Rehmeier, Polym. Degrad. Stab. 90 (3) (2005) 471–480.
[11] A.N. Chaudhry, N.C. Billingham, Polym. Degrad. Stab. 73 (3) (2001) 505–510.
[12] B.H. Youn, C.S. Huh, IEEE Trans. Dielect. Elect. Insul. 12 (5) (2005) 1015–1024.
[13] H. Liu, G. Cash, D. Birtwhistle, G. George, IEEE Trans. Dielect. Elect. Insul. 12 (3) (2005) 478–486.
[14] T.G. Gustavsson, S.M. Gubanski, H. Hillborg, S. Karlsson, U.W. Gedde, IEEE Trans. Dielect. Elect. Insul. 8 (6) (2001) 1029–1039.
[15] D. Graiver, K.W. Farminer, R. Narayan, J. Polym. Environ. 11 (4) (2003) 129–136.
[16] J. Tan, Y.J. Chao, J.W. Van Zee, W.K. Lee, Mater. Sci. Eng. A 445/446 (2007) 669–675.
[17] J. Tan, Y.J. Chao, M. Yang, C.T. Williams, J.W. Van Zee, J. Mater. Eng. Perform., submitted for publication.
[18] N. Yoshimura, S. Kumagai, S. Nishimura, IEEE Trans. Dielect. Elect. Insul. 6 (5) (1999) 632–650.
[19] F. Delor-Jestin, N.S. Tomer, R.P. Singh, J. Lacoste, E-Polymer 5 (2006) 1–13.
[20] D. Lin-Vien, N.B. Colthup, W.G. Fateley, J.G. Grasselli, The Handbook of Infrared and Raman Characteristic Frequencies of Organic Molecules, Academic Press, Boston, 1991.
[21] W. Noll, Chemistry and Technology of Silicone, Academic Press, Boston, 1968.
[22] E.W. Colvin, Silicone in Organic Synthesis, Butterworth and Co. (Publishers) Ltd., Butterworths, 1981.
[23] A. Streiwieser Jr., C.H. Heathcock, Introduction to Organic Chemistry, Macmillican Publishing Co., New York, 1976.
[24] X. Li, Y.H. An, Y.D. Wu, Y.C. Song, Y.J. Chao, C.H. Chien, J. Biomed. Mater. Res., Part B: Appl. Biomater. (2006) 25–31.
[25] Y.Y. Lim, M. Munawar Chaudhri, Mech. Mater. 38 (2006) 1213–1228.
[26] K.L. Johnson, Contact Mechanics, Cambridge University Press, Cambridge, 1985.